OPEN ACCESS Freely available online

PLoS one

Distinct RGK GTPases Differentially Use α_1- and Auxiliary β-Binding-Dependent Mechanisms to Inhibit $Ca_V1.2$/$Ca_V2.2$ Channels

Tingting Yang*, Akil Puckerin, Henry M. Colecraft*

Department of Physiology and Cellular Biophysics, Columbia University, College of Physicians and Surgeons, New York, New York, United States of America

Abstract

Ca_V1/Ca_V2 channels, comprised of pore-forming α_1 and auxiliary (β,$\alpha_2\delta$) subunits, control diverse biological responses in excitable cells. Molecules blocking Ca_V1/Ca_V2 channel currents (I_{Ca}) profoundly regulate physiology and have many therapeutic applications. Rad/Rem/Rem2/Gem GTPases (RGKs) strongly inhibit Ca_V1/Ca_V2 channels. Understanding how RGKs block I_{Ca} is critical for insights into their physiological function, and may provide design principles for developing novel Ca_V1/Ca_V2 channel inhibitors. The RGK binding sites within Ca_V1/Ca_V2 channel complexes responsible for I_{Ca} inhibition are ambiguous, and it is unclear whether there are mechanistic differences among distinct RGKs. All RGKs bind β subunits, but it is unknown if and how this interaction contributes to I_{Ca} inhibition. We investigated the role of RGK/β interaction in Rem inhibition of recombinant $Ca_V1.2$ channels, using a mutated β (β_{2aTM}) selectively lacking RGK binding. Rem blocked β_{2aTM}-reconstituted channels (74% inhibition) less potently than channels containing wild-type β_{2a} (96% inhibition), suggesting the prevalence of both β-binding-dependent and independent modes of inhibition. Two mechanistic signatures of Rem inhibition of $Ca_V1.2$ channels (decreased channel surface density and open probability), but not a third (reduced maximal gating charge), depended on Rem binding to β. We identified a novel Rem binding site in $Ca_V1.2$ α_{1C} N-terminus that mediated β-binding-independent inhibition. The $Ca_V2.2$ α_{1B} subunit lacks the Rem binding site in the N-terminus and displays a solely β-binding-dependent form of channel inhibition. Finally, we discovered an unexpected functional dichotomy amongst distinct RGKs— while Rem and Rad use both β-binding-dependent and independent mechanisms, Gem and Rem2 use only a β-binding-dependent method to inhibit $Ca_V1.2$ channels. The results provide new mechanistic perspectives, and reveal unexpected variations in determinants, underlying inhibition of $Ca_V1.2$/$Ca_V2.2$ channels by distinct RGK GTPases.

Citation: Yang T, Puckerin A, Colecraft HM (2012) Distinct RGK GTPases Differentially Use α_1- and Auxiliary β-Binding-Dependent Mechanisms to Inhibit $Ca_V1.2$/$Ca_V2.2$ Channels. PLoS ONE 7(5): e37079. doi:10.1371/journal.pone.0037079

Editor: J. David Spafford, University of Waterloo, Canada

Received February 14, 2012; **Accepted** April 13, 2012; **Published** May 10, 2012

Funding: This work was supported by grants to HMC from the National Institutes of Health (RO1 HL069911 and RO1 HL084332). HMC is an Established Investigator of the American Heart Association. The funders had no role in study design, data collection and analysis, decision to publish, or preparation of the manuscript.

Competing Interests: The authors have declared that no competing interests exist.

* E-mail: hc2405@columbia.edu (HMC); ty2190@columbia.edu (TY)

Introduction

Ca^{2+} influx via high-voltage-activated Ca_V1/Ca_V2 Ca^{2+} channels links electrical signals to physiological responses in excitable cells, and consequently, regulates myriad biological functions ranging from muscle contraction to hormone and neurotransmitter release [1,2]. Ca_V1/Ca_V2 channel activity is modulated by various intracellular signaling molecules, and this serves as a powerful method to alter physiology [1,3]. Furthermore, molecules that selectively inhibit Ca_V1/Ca_V2 channels are current or prospective therapeutics for serious cardiovascular (e.g. hypertension, angina) and neurological (e.g. Parkinson's disease, neuropathic pain, stroke) diseases [4,5,6,7,8].

Rad/Rem/Rem2/Gem (RGK) proteins are a four-member subfamily of the Ras superfamily of monomeric GTPases [9], and are the most potent known intracellular inhibitors of Ca_V1/Ca_V2 channels [10,11,12]. RGK proteins are present in excitable tissue— including skeletal/cardiac muscle, nerve, and endocrine cells— suggesting that their inhibition of Ca_V1/Ca_V2 channels has physiological significance. Consistent with this notion, suppression of basal Rad expression in heart increases L-type $Ca_V1.2$ calcium current ($I_{Ca,L}$) and leads to cardiac hypertrophy [13,14]. Mechanistically, RGK GTPases inhibit Ca_V1/Ca_V2 channels using multiple methods [15]. For example, Rem inhibits recombinant $Ca_V1.2$ channels reconstituted in HEK 293 cells using at least three independent mechanisms [16]: (1) by decreasing the number of channels (N) at the cell surface; (2) by inhibiting open probability (P_o) of surface channels; and (3) by partially immobilizing voltage sensors as reported by a reduced maximal gating charge (Q_{max}).

A core unanswered question relates to the geographical localization of RGK binding site(s) on Ca_V1/Ca_V2 channel complexes responsible for I_{Ca} inhibition. Mature Ca_V1/Ca_V2 channels are macro-molecular complexes comprised minimally of a pore-forming α_1 protein assembled with auxiliary $\beta/\alpha_2\delta$ subunits, and calmodulin [2,17]. $Ca_V\beta$ is required for α_1 trafficking to the plasma membrane, enhancing channel open probability (P_O), and normalizing channel gating [18,19]. All four RGKs bind $Ca_V\beta$s and it has been widely assumed, though not proven, that the RGK/β interaction is essential for Ca_V1/Ca_V2 channel inhibition [10,12,15,20]. This notion has been strongly

challenged by a recent finding that β binding is not necessary for Gem inhibition of neuronal P/Q-type ($Ca_V2.1$) channels [21]. This new provocative result raises several outstanding fundamental questions. First, it is now unclear whether the RGK/β interaction plays any role in I_{Ca} inhibition, or whether it is merely an unrelated epi-phenomenon. Second, though it has been proposed that RGKs may inhibit Ca_V1/Ca_V2 channels by binding directly to pore-forming α_1 subunits [21,22], to date no RGK binding site responsible for I_{Ca} reduction has been described for any α_1-subunit isoform. Third, while it is formally possible that distinct RGKs may use different mechanisms and determinants to inhibit individual Ca_V1/Ca_V2 channels, this idea has not been explored.

Here, we report that Rem uses both β-binding-dependent and β-binding-independent mechanisms to inhibit recombinant $Ca_V1.2$ channels. We identified a novel Rem binding region on the N-terminus of the pore-forming $Ca_V1.2$ α_{1C} subunit that mediates β-binding-independent inhibition. The N-type ($Ca_V2.2$) channel α_{1B} subunit lacks the Rem binding site in the N-terminus and displays only β-binding-dependent inhibition. Finally, we discovered that distinct RGK GTPases differ in their use of the two determinants for $Ca_V1.2$ channel suppression— Rem and Rad use both β-binding-dependent and independent mechanisms, whereas Gem and Rem2 solely utilize a β-binding-dependent mode of inhibition.

Results

Rem inhibits $Ca_V1.2$ channels using both β-binding-dependent and β-binding-independent mechanisms

Rem potently inhibits recombinant $Ca_V1.2$ channels (α_{1C}/β_{2a}) reconstituted in HEK 293 cells (Fig. 1 B and C). Cells transiently transfected with α_{1C}+β_{2a} generate robust $I_{Ca,L}$ which is virtually eliminated (96% inhibition) when Rem is co-expressed (Fig. 1 B and C). It is unknown whether this dramatic effect is mediated through Rem binding to the auxiliary β, the pore-forming α_{1C} subunit, or both (Fig. 1A). To address this issue, we introduced three point mutations (D243A, D319A and D321A) into β_{2a} to generate a mutant (β_{2aTM}) that selectively loses binding to RGK proteins, as previously demonstrated [23] and confirmed here (Fig. S1). Cells expressing mutant $Ca_V1.2$ channels reconstituted with α_{1C}+β_{2aTM} yielded strong $I_{Ca,L}$ with amplitude and voltage-dependence indistinguishable from wild-type $Ca_V1.2$ (Fig. 1 D and E), demonstrating that the mutations did not adversely affect the structure and functional interaction of β with α_{1C}. Rem inhibited $I_{Ca,L}$ through mutant α_{1C}+β_{2aTM} $Ca_V1.2$ channels (Fig. 1 D and E). However, the magnitude of Rem inhibition of mutant channels (74%) was significantly less than observed with wild type $Ca_V1.2$ (Fig. 1). The intermediate impact of Rem on α_{1C}+β_{2aTM} channels indicates Rem inhibits $Ca_V1.2$ channels using both β-binding-dependent and independent mechanisms.

We previously reported that Rem inhibits $Ca_V1.2$ channels using multiple, independent methods: decreasing N, P_o, and Q_{max} [16]. We investigated which, if any, of these distinct mechanisms is dependent on Rem binding to β. To quantitatively determine the relative $Ca_V1.2$ surface density we introduced a 13-residue high-affinity bungarotoxin (BTX) binding site (BBS) into the extracellular domain II S5–S6 loop in α_{1C}-YFP [16]. Surface α_{1C}[BBS]-YFP was detected in non-permeabilized cells by sequential exposure to biotinylated BTX and streptavidin-conjugated quantum dot (QD). Labeled cells are then subject to flow cytometry, permitting high throughput measurements of fluorescence signals [16,24] (Fig. S2). Cells expressing α_{1C}[BBS]-YFP+β_{2a} displayed a strong QD_{655} fluorescence signal (Fig. 2A, *top row*), indicating an abundance of channels at the cell surface. Co-expression of CFP-Rem with wild-type $Ca_V1.2$ markedly decreased N, as reported by a ~75% decrease in mean QD_{655} fluorescence (Fig. 2A; normalized mean QD_{655} fluorescence = 0.26±0.01, n = 3 independent flow cytometry experiments in cells co-expressing CFP-Rem compared to control cells expressing α_{1C}[BBS]-YFP+β_{2a} alone). These results are consistent with our previous observations [16]. Cells expressing α_{1C}[BBS]-YFP+β_{2aTM} displayed a similar channel surface density as control α_{1C}[BBS]-YFP+β_{2a} cells (Fig. 2B; normalized mean QD_{655} fluorescence = 0.94±0.04, n = 3). Interestingly, CFP-Rem barely decreased QD_{655} fluorescence in cells expressing α_{1C}[BBS]-YFP+β_{2aTM} (Fig. 2B; normalized mean QD_{655} fluorescence = 0.77±0.02, n = 3), compared to the substantial drop observed with control channels (Fig. 2A). Therefore, the ability of Rem to reduce N is critically dependent on its capacity to bind β.

A second mode of Rem inhibition of $Ca_V1.2$ involves a reduction in channel P_o that depends on membrane targeting of Rem's nucleotide binding domain (NBD) [16,20]. When expressed in cells, wild-type Rem autonomously targets to the inner leaflet of the plasma membrane via electrostatic and hydrophobic interactions afforded by basic and aromatic residues in the distal C-terminus [25]. A Rem truncation mutant, Rem_{265}, featuring a deletion of the final 32 amino acid residues in the C-terminus, loses both membrane targeting and the ability to block I_{Ca} [12,16,20]. Replacing the deleted 32 residues with a generic membrane-targeting domain rescues the capacity to inhibit I_{Ca} [26]. We exploited this feature to generate an inducible Ca_V channel inhibitor by placing the C1 domain of protein kinase Cγ (PKCγ) to the end of CFP-Rem_{265} [16]. When expressed in cells, the resulting construct, CFP-Rem_{265}-$C1_{PKC}$, is cytosolic but can be rapidly recruited to the plasma membrane with the phorbol ester, PdBu (Fig. 2C). In α_{1C}+β_{2a} channels, membrane recruitment of Rem_{265}-$C1_{PKC}$ results in an attendant rapid and substantive 60% decrease in I_{Ca} (Fig. 2D), which is solely due to a decrease in P_o [16,20]. In sharp contrast, α_{1C}+β_{2aTM} channels were unaffected by membrane-recruitment of Rem_{265}-$C1_{PKC}$ (Fig. 2E). The slight 10% reduction in I_{Ca} observed in this group is commensurate with the normal amount of channel rundown observed in these time course experiments. These results establish that this Rem-induced reduced-P_o mechanism of channel inhibition is also mediated through the Rem/β interaction.

A third characteristic functional impact of Rem on $Ca_V1.2$ channels is a reduction of Q_{max} that occurs even when the decrease in N is accounted for, and is likely accomplished by a Rem-induced partial immobilization of α_{1C} voltage sensors [16]. Wild-type α_{1C}+β_{2a} channels yield large ON gating currents and Q_{max}, which are almost eliminated in the presence of CFP-Rem (Fig. 2F). Qualitatively similar results were obtained with mutant α_{1C}+β_{2aTM} channels, which displayed a large Q_{max} that was significantly reduced by CFP-Rem (Fig. 2G). Therefore, unlike the effects on N and P_o, binding to β is not necessary for Rem-induced decrease of $Ca_V1.2$ Q_{max}.

Identification of a novel Rem binding region on the pore-forming α_{1C} subunit

The most parsimonious explanation for the existence of a β-binding-independent mode of Rem-induced block of $I_{Ca,L}$ is that Rem directly binds α_{1C} to initiate this form of $Ca_V1.2$ inhibition. However, to date, no such functional Rem binding site on α_{1C} has been described. Given that Rem is localized to the intracellular side of the plasma membrane, we hypothesized the existence of a Rem binding site somewhere within the major cytoplasmic regions (N-terminus, I–II loop, II–III loop, III–IV loop, and C-terminus)

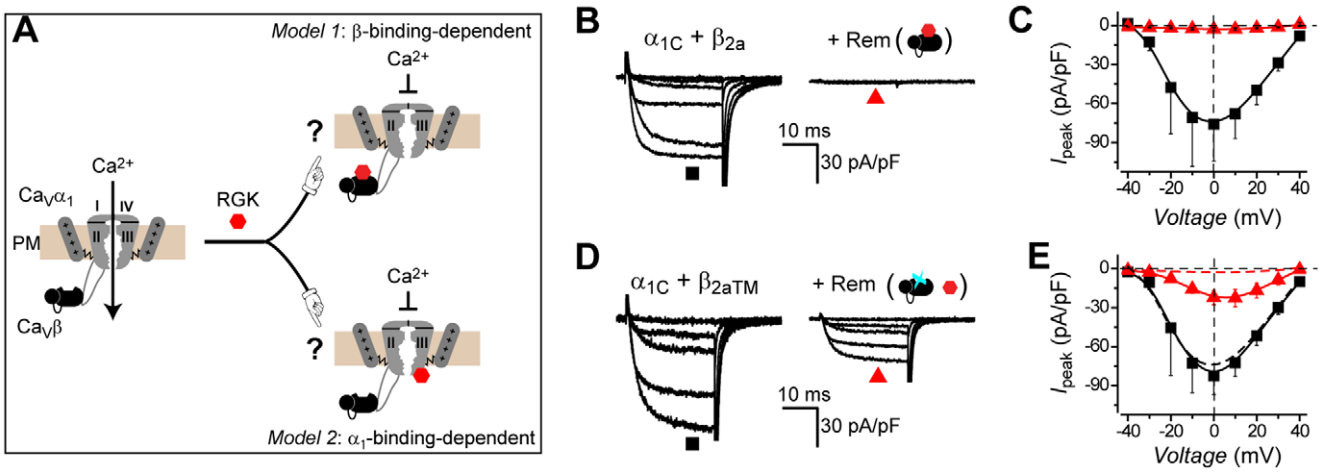

Figure 1. Rem inhibits $Ca_V1.2$ channels using both β-binding-dependent and independent mechanisms. (A) Alternative models for Rem functional interaction with $Ca_V1.2$ channel complex. (B) Exemplar Ba^{2+} currents from HEK 293 cells expressing wild-type $Ca_V1.2$ (α_{1C}+β_{2a}) in the absence (*left*) or presence (*right*) of Rem. (C) Population current density (I_{peak}) vs. voltage relationships for wild-type $Ca_V1.2$ channels in the absence (■, $n = 6$ for each point) or presence (red ▲, $n = 5$ for each point) of Rem. Data are means ± S.E.M. (D, E) Data for mutant $Ca_V1.2$ channels (α_{1C}+β_{2aTM}) in the absence (■, $n = 8$ for each point) or presence (red ▲, $n = 10$ for each point) of Rem. Same format as B, C. In *E*, data from wild-type $Ca_V1.2$ channels are reproduced (dotted lines) to facilitate direct visual comparison.
doi:10.1371/journal.pone.0037079.g001

of α_{1C} (Fig. 3A). We searched for such a binding site using two complementary methods. First, we used fluorescence resonance energy transfer (FRET) to probe for an interaction between YFP-Rem and CFP-tagged intracellular domains of α_{1C} (Fig. 3B). Using a three-cube FRET method [27,28], we found that only CFP-tagged α_{1C} N-terminus (CFP-α_{1C}NT) yielded an appreciable FRET signal when co-expressed with YFP-Rem (Fig. 3B). None of the other CFP-tagged α_{1C} intracellular loops yielded a FRET signal significantly above control cells expressing YFP-Rem+CFP (Fig. 3B, dotted line). The FRET results were not due to differences in the stoichiometry of donor to acceptor molecules since the estimated ratio of donor (N_D) to acceptor (N_A) molecules [27,28] was similar among the different groups (Fig. S3). The FRET results aligned with visual evidence of protein co-localization (Fig. 3). When expressed individually, YFP-Rem is enriched at the plasma membrane whereas CFP-α_{1C}NT has a mostly diffuse fluorescence through the cytosol and in the nucleus (Fig. S4). However, when co-expressed with YFP-Rem, a fraction of the CFP-α_{1C}NT present in cells was targeted to the plasma membrane, tracking the membrane localization of Rem and providing visual evidence of an interaction (Fig. 3B; Fig. S4).

As a complementary approach, we used co-immunoprecipitation (co-IP) assays to determine interaction between YFP-Rem and individual CFP-tagged α_{1C} intracellular domains co-transfected into HEK 293 cells (Fig. 3C). All CFP-tagged α_{1C} intracellular domains and YFP-Rem were well expressed (Fig. 3C, *input*). Only CFP-α_{1C}NT co-IPed with YFP-Rem (Fig. 3C), corroborating the results from FRET and protein co-localization approaches (Fig. 3B). As a further control experiment, we observed no pull down of CFP-α_{1C}NT with anti-Rem antibody in cells transfected with CFP-α_{1C}NT alone (*i.e.*, no YFP-Rem co-expressed; not shown). We were surprised to find no binding between Rem and α_{1C} C-terminus (α_{1C}CT) given a recent report that these two proteins interact [29]. The reasons for this disparity are unclear. However, the fact that using three independent approaches (FRET, co-localization analyses, and co-IP) we could observe no interaction between Rem and α_{1C}CT while detecting association with α_{1C}NT effectively rules out the potential trivial explanation of a false negative result that could conceivably be obtained with any one method. One possibility is that the presence of fluorescent protein tags on Rem and α_{1C}CT may occlude or weaken this interaction to a point where it is undetectable in our different assay conditions.

α_{1C}NT is comprised of 153 amino acid residues. Peptide mapping (Fig. 3D) combined with co-IP (Fig. 3E) and confocal co-localization (Fig. S5) experiments suggested the Rem binding site resides in a region towards the distal end of α_{1C}NT. This region is immediately upstream of transmembrane segment 1 in domain I (IS1), and shows homology (60% identical residues or conservative substitutions) among distinct Ca_V1/Ca_V2 α_1-subunit isoforms (Fig. 3F). Surprisingly, despite the high sequence homology, Rem did not bind $Ca_V2.2$ N-terminus (α_{1B}NT) as determined either by FRET (Fig. 4A) or visual inspection of protein co-localization (not shown).

Rem association with α_{1C}NT mediates β-binding-independent inhibition of $Ca_V1.2$

Does Rem binding to α_{1C}NT mediate β-binding-independent $Ca_V1.2$ inhibition? We addressed this question in several ways. First, given that $Ca_V2.2$ α_{1B}NT does not bind Rem (nor do any of the other α_{1B} intracellular domains) (Fig. 4A), we hypothesized that $Ca_V2.2$ would lack a β-binding-independent form of channel inhibition. Indeed, while Rem strongly suppressed I_{Ca} in control cells expressing α_{1B}+β_{2a} (Fig. 4B), it had no impact on α_{1B}+β_{2aTM} channels (Fig. 4C). Hence, Rem inhibits $Ca_V2.2$ channels solely through a β-binding-dependent mechanism. We attempted to exchange N-termini between $Ca_V1.2$ α_{1C} and $Ca_V2.2$ α_{1B}, to determine if α_{1C}NT is necessary and sufficient to reconstitute β-binding-independent Rem inhibition in Ca_V1/Ca_V2 channel α_1 subunits. Unfortunately, the chimeric channels gave rise to very small currents suggesting that α_1-subunit N-termini may have a customized, non-transferable role in the structural and/or functional maturation of individual Ca_V1/Ca_V2 channels.

As an alternative approach towards evaluating the functional importance of Rem/a_{1C}NT association, we determined the impact of over-expressing α_{1C}NT on Rem inhibition of α_{1C}+β_{2a} and α_{1C}+β_{2aTM} channels, respectively. We reasoned that if Rem/

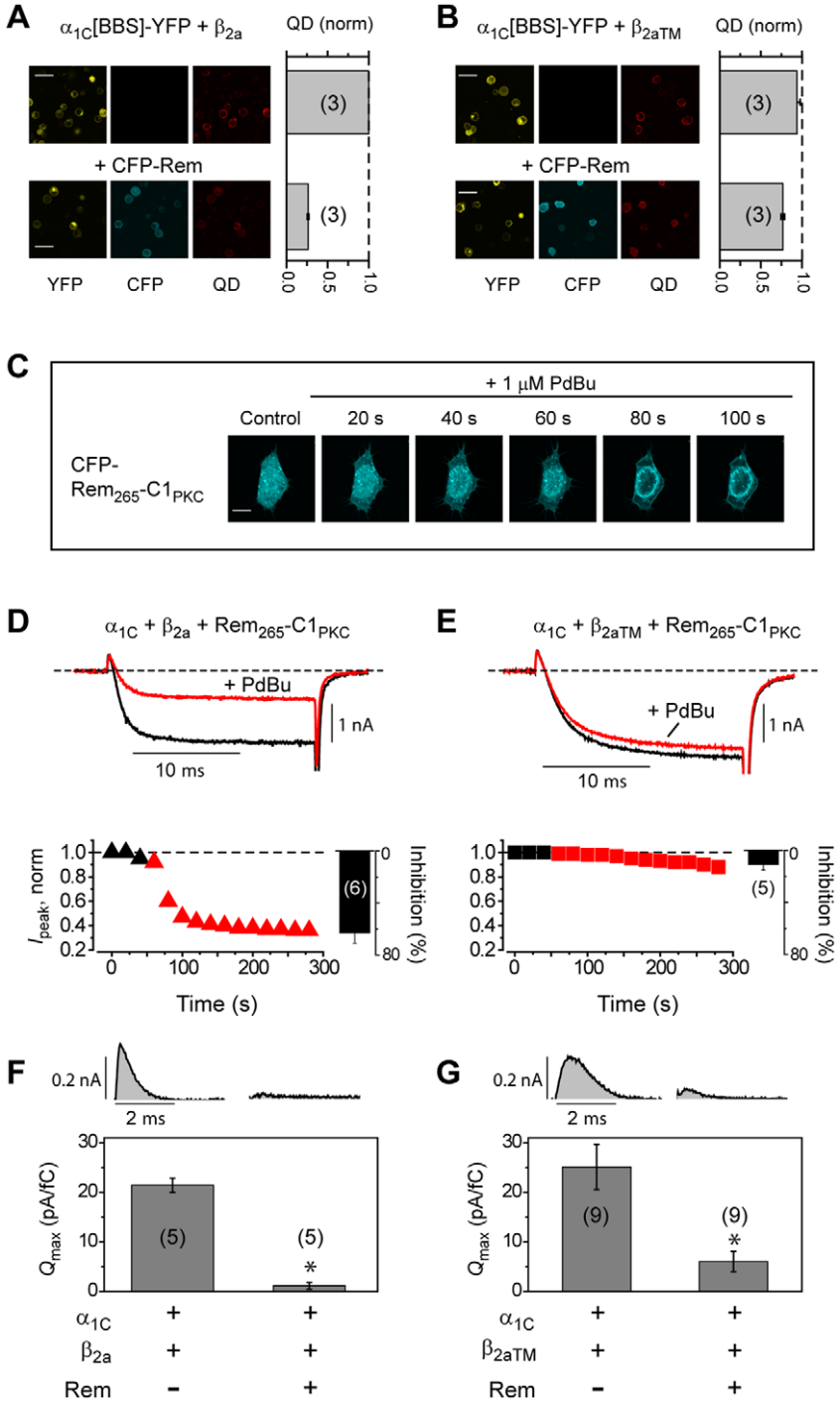

Figure 2. Distinct mechanisms of Rem inhibition of $Ca_V1.2$ differentially depend on Rem/β interaction. (A, B) Differential impact of CFP-Rem on surface density of wild-type (α_{1C}[BBS]-YFP+β_{2a}) and mutant (α_{1C}[BBS]-YFP+β_{2aTM}) $Ca_V1.2$ channels, respectively, using a surface channel quantum dot labeling method. Confocal images for corresponding imaging channels were obtained with identical instrument settings. Scale bar, 25 μm. (C) Rapid recruitment of CFP-Rem_{265}-$C1_{PKC}$ to the plasma membrane induced by 1 μM PdBu. Scale bar, 8 μm. (D, E) PdBu-induced membrane translocation of CFP-Rem_{265}-$C1_{PKC}$ concomitantly inhibits wild-type (α_{1C}+β_{2a}), but not mutant (α_{1C}+β_{2aTM}) $Ca_V1.2$ channels. (F, G) Rem inhibits gating currents and Q_{max} in both wild-type and mutant $Ca_V1.2$ channels. * $P<0.05$ when compared to the corresponding without Rem data using Student's two-tailed unpaired *t* test.
doi:10.1371/journal.pone.0037079.g002

α_{1C}NT interaction is functionally relevant then over-expressing α_{1C}NT would, via competition, partially rescue Rem inhibition of α_{1C}+β_{2a} channels, while fully overcoming Rem inhibition of α_{1C}+β_{2aTM} channels (Fig. 4D). Indeed, these predictions were borne out in functional experiments. Over-expressing α_{1C}NT partially relieved Rem inhibition of wild type $Ca_V1.2$ channels (Fig. 4E; $I_{peak,0mV} = 20.9 \pm 5.4$ pA/pF, $n = 6$ for cells expressing α_{1C}+β_{2a}+Rem+α_{1C}NT compared to $I_{peak,0mV} = 2.8 \pm 1.2$ pA/pF,

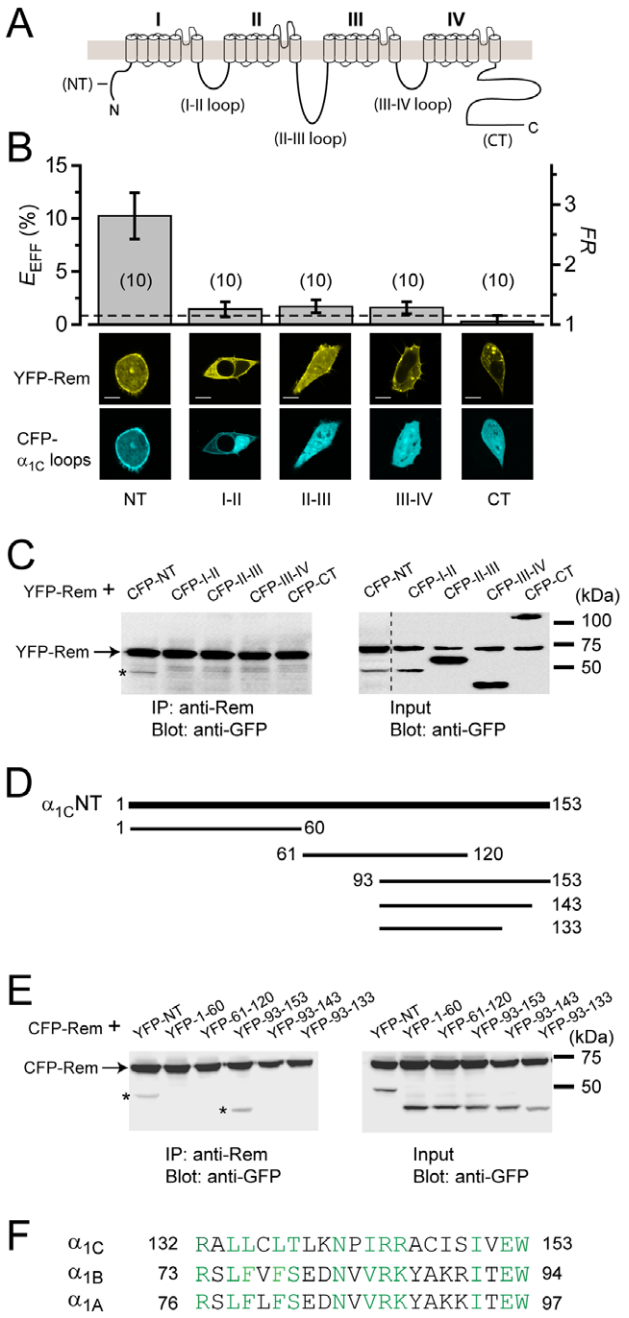

Figure 3. Rem binds α_{1C} N-terminus. (A) Schematic of α_{1C} showing four homologous transmembrane domains (I–IV), intracellular N/C termini and domain-connecting loops. (B) *Top*, interaction of individual CFP-tagged α_{1C} intracellular loops and termini with YFP-Rem probed using FRET. Dotted line represents YFP-Rem+CFP ($n = 10$). *Bottom*, confocal images. Scale bar, 8 μm. (C) CFP-tagged α_{1C}NT co-immunoprecipitates with YFP-Rem. All the co-ip lanes and the first input lane were from the same gel. The rest of the input lanes were from a second gel run simultaneously because there were insufficient lanes available in the first gel to accommodate all samples, including marker lanes. Hence, in the input gel image (*right*) the first lane (CFP-NT) was spliced onto the rest of the lanes (dotted line). The co-ip gels have been cropped to remove light chain IgG bands from the precipitating antibody. (D) Schematic of α_{1C}NT peptide fragments. (E) Co-immunoprecipitation of YFP-tagged α_{1C}NT peptide fragments with CFP-Rem. (F) Sequence comparison of last 22 N-terminus residues among distinct Ca_V1/Ca_V2 channel α_1 subunits.
doi:10.1371/journal.pone.0037079.g003

$n = 5$ for α_{1C}+β_{2a}+Rem, $P<0.05$, Student's t test), while fully rescuing mutant channel currents (Fig. 4E; $I_{peak,0mV} = 80.1 \pm 23.5$ pA/pF, $n = 8$ for cells expressing α_{1C}+β_{2aTM}+Rem+α_{1C}NT compared to $I_{peak,0\ mV} = 92.4 \pm 15.5$ pA/pF, $n = 8$ for cells α_{1C}+β_{2aTM}). As a control experiment, α_{1B}NT had no impact on Rem inhibition of mutant channels (Fig. 4E; $I_{peak,0\ mV} = 18.2 \pm 4.6$ pA/pF, $n = 5$ for cells expressing α_{1C}+β_{2aTM}+Rem+α_{1B}NT compared to $I_{peak,0\ mV} = 22.2 \pm 5.3$ pA/pF, $n = 10$ for α_{1C}+β_{2aTM}+Rem). These results are consistent with the idea that Rem/α_{1C}NT association mediates β-binding-independent Rem inhibition of $Ca_V1.2$ channels.

Distinct RGK GTPases differentially use α_1- and β-binding dependent mechanisms to inhibit $Ca_V1.2$ channels

We next examined whether the use of both α_1- and β-binding mechanisms to inhibit $Ca_V1.2$ channels is a conserved feature among the four distinct RGK GTPases. Initial indications of fundamental differences were immediately apparent from visual confocal co-localization images and co-immunoprecipitation experiments which demonstrated that unlike Rem, none of the other RGK proteins— Gem, Rem2, and Rad— bound α_{1C}NT (Fig. S6). We assessed the impact of individual RGKs on either α_{1C}+β_{2a} or α_{1C}+β_{2aTM} channels reconstituted in HEK 293 cells, and observed a sharp dichotomy in functional responses (Fig. 5A). Whereas, all RGKs markedly inhibited $I_{Ca,L}$ through wild-type α_{1C}+β_{2a} channels only Rem and Rad also inhibited α_{1C}+β_{2aTM} channels. Mutant α_{1C}+β_{2aTM} channels were completely refractory to Gem and Rem2, explicitly demonstrating that these RGK proteins utilize only β-binding-dependent mechanisms to inhibit $I_{Ca,L}$ (Fig. 5 A and B). The finding that Rad displayed both a β-binding-dependent and a β-binding-independent mode of inhibition (albeit to a lesser extent than observed for Rem) was surprising given its apparent lack of binding to α_{1C} N-terminus (Fig. S6). We speculated that Rad may bind to another intracellular domain of α_{1C} to initiate β-binding-independent inhibition of $Ca_V1.2$. However, we could not detect any evidence of Rad binding to any of the other major intracellular domains of α_{1C} (Fig. S7). One possibility is that Rad may bind to α_{1C} using multiple weak interactions rather than a dominant strong binding site as we have found for Rem.

Discussion

Amongst the myriad forms of physiological modulation of Ca_V channels by intracellular signaling molecules, inhibition of Ca_V1/Ca_V2 channels by RGKs stands out for its potency (often virtual elimination of I_{Ca}) and indiscrimination (affects all Ca_V1/Ca_V2 isoforms). In this regard, RGKs behave as polar opposites to Ca_V channel auxiliary β subunits which interact promiscuously with all Ca_V1/Ca_V2 to stimulate I_{Ca} by increasing channel membrane trafficking and increasing single-channel open probability (P_o). Given this fact, the discovery that RGKs bind βs led to the widely-held assumption that RGK/β interaction was fundamental to the mechanism of channel inhibition [15,30]. Early renditions of this idea suggested that RGKs bound to βs and prevented their interaction with α_1 subunits, thereby compromising channel trafficking to the membrane [10,31,32], and leaving channels at the cell surface in a low-P_o 'α_1-alone' mode [33]. However, it was subsequently shown that RGKs do not disrupt the α_1-β interaction leading to revised models invoking a ternary α_1/β/RGK complex in which βs bridge α_1 subunits and RGKs to initiate I_{Ca} inhibition [11,16,20,34,35]. Recently, the primacy of the RGK/β interaction in the mechanism of I_{Ca} inhibition has been challenged based on the interesting finding that preventing Gem interaction with β did

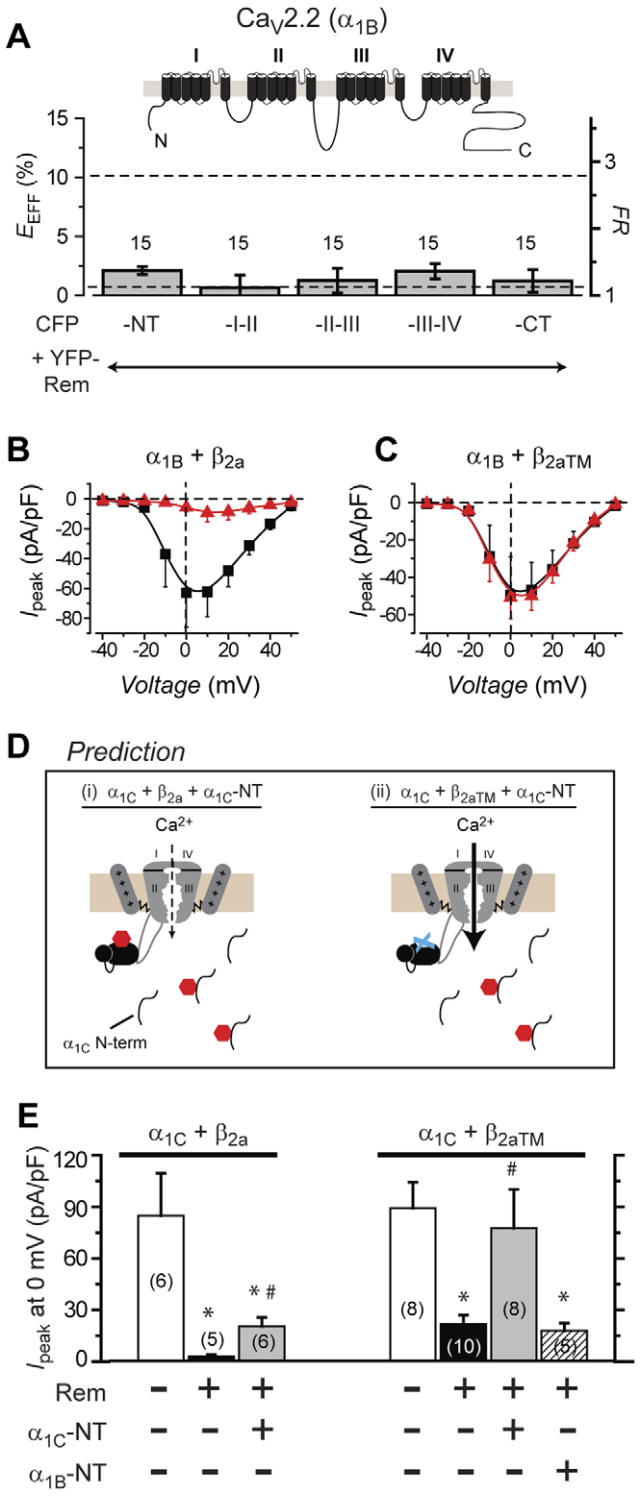

Figure 4. Rem interaction with α_{1C} N-terminus mediates β-binding-independent inhibition. (A) *Top*, topography of $Ca_V2.2$ α_{1B} subunit. *Bottom*, interaction of $Ca_V2.2$ α_{1B} intracellular domains with YFP-Rem probed using FRET. Dotted lines represent FRET data from YFP-Rem+CFP-α_{1C}NT and YFP-Rem+CFP, respectively. (B, C) Population I_{peak}-V relationships for wild type (α_{1B}+β_{2a}) and mutant (α_{1B}+β_{2aTM}) $Ca_V2.2$ channels, respectively, in the absence (■, $n=5$ for wild type channels, and $n=9$ for mutant channels) or presence (red ▲, $n=5$ for wild type channels, and $n=10$ for mutant channels) of Rem. Data are means ± S.E.M. (D) Schematic showing rationale and predictions for α_{1C} N-terminus over-expression experiments. (E) Histogram showing impact of α_{1C} or α_{1B} N-terminus on wild-type (α_{1C}+β_{2a}) and mutant (α_{1C}+β_{2aTM}) $Ca_V1.2$ channels in the presence of Rem. * $P<0.05$ when compared to α_{1C}+β_{2a} or α_{1C}+β_{2aTM} using two-tailed unpaired Student's t test. # $P<0.05$ when compared to α_{1C}+β_{2a}+Rem or α_{1C}+β_{2aTM}+Rem using two-tailed unpaired Student's t test.
doi:10.1371/journal.pone.0037079.g004

not impair its ability to block $Ca_V2.1$ (P/Q) channels [21]. In the wake of this report, it is unclear whether the RGK/β interaction has any role in the mechanism of I_{Ca} inhibition, or merely represents an unrelated epiphenomenon. We have investigated this issue using a β_{2a}-subunit mutant that selectively loses binding to RGK proteins. The new findings presented in this work are: (1) Rem inhibits $Ca_V1.2$ channels using both β-binding-dependent and β-binding–independent mechanisms; (2) binding to β is required for Rem-mediated decrease in $Ca_V1.2$ channel surface density (N) and open probability (P_o), but not Q_{max}; (3) Rem associates with α_{1C} N-terminus to initiate β-binding-independent inhibition; (4) Rem inhibits $Ca_V2.2$ channels using a solely β-binding-dependent mechanism; (5) distinct RGKs differentially use β-binding-dependent and α_1-binding-dependent mechanisms to inhibit Ca_V1/Ca_V2 channels.

The finding that all four RGKs use (at least partially) β-binding-dependent mechanisms to suppress $Ca_V1.2$ channels, reasserts the importance of the RGK/β interaction for I_{Ca} inhibition. Indeed, for Gem and Rem2, a β-binding-dependent mechanism was the sole mode for inhibiting $Ca_V1.2$ channels. Similarly, Rem inhibited $Ca_V2.2$ channels solely through a β-binding-dependent

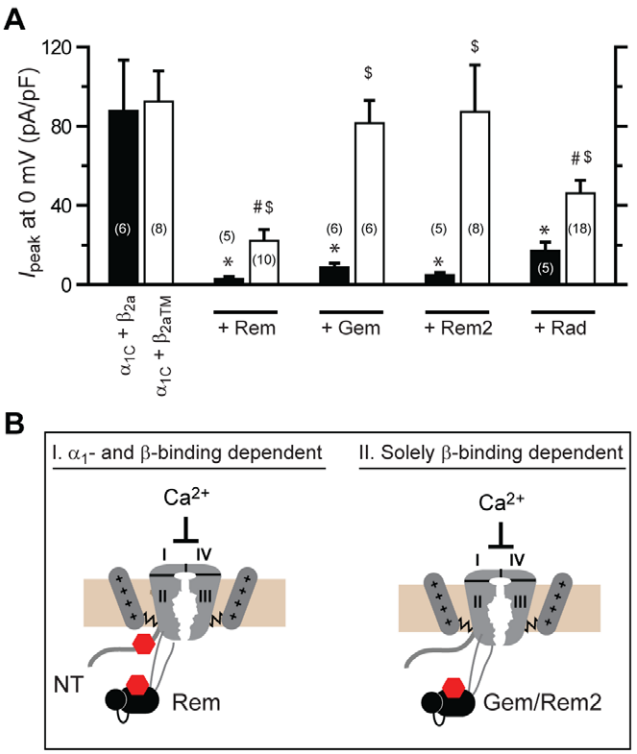

Figure 5. Distinct RGKs differentially use β-binding-dependent and independent mechanisms to inhibit $Ca_V1.2$ channels. (A) Histogram showing impact of individual RGKs on wild-type (α_{1C}+β_{2a}) and mutant (α_{1C}+β_{2aTM}) $Ca_V1.2$ channels. *, #, $ $P<0.05$ when compared to α_{1C}+β_{2a}, α_{1C}+β_{2aTM}, or α_{1C}+β_{2a}+RGK, respectively, using two-tailed unpaired Student's t test. (B) Cartoon showing dichotomy in the determinants used by distinct RGKs to inhibit $Ca_V1.2$ channels.
doi:10.1371/journal.pone.0037079.g005

mechanism, indicating this phenomenon is not limited to just $Ca_V1.2$ channels. Beyond β-binding-dependent inhibition, Rem and Rad also blocked $Ca_V1.2$ channels in a β-binding-independent manner. For Rem, this response was mediated through an association with α_{1C}NT. The discovery of an α_{1C}-binding-dependent mode of RGK inhibition in $Ca_V1.2$ channels aligns with the finding that Gem inhibits $Ca_V2.1$ channels in a β-binding-independent (and presumably α_{1A}-binding-dependent) manner [21]. Taken together with previous studies [21,22], our data suggests a dualistic view for RGK regulation of $Ca_V1.2$ channels. First, all RGKs can inhibit Ca_V1/Ca_V2 channels by interacting with β subunits. The essential role of βs in the functional maturation of all Ca_V1/Ca_V2 channels may, therefore, explain the indiscriminate nature of RGK inhibition of I_{Ca} through HVA Ca_V channels. Second, distinct RGKs can selectively inhibit specific Ca_V1/Ca_V2 channel isoforms by differentially binding to individual α_1 subunits. This insight may be potentially exploited to engineer RGKs with sole selectivity for individual α_1 subunits as a means of creating custom, isoform-specific genetically encoded Ca_V1/Ca_V2 channel inhibitors [17]. For Rem inhibition of $Ca_V1.2$, the α_{1C}-binding-dependent and β-binding-dependent mechanisms appear to be equally potent in blocking $I_{Ca,L}$.

How does binding of RGK proteins to either β or α_1 subunits actually suppress I_{Ca}? Rem inhibition of recombinant $Ca_V1.2$ channels occurs via multiple mechanisms including: decreased N (due to enhanced dynamin-dependent endocytosis), P_o, and Q_{max} (due to voltage sensor immobilization) [16]. Interestingly, Rem-induced decrease in N and P_o (but not Q_{max}) was β-binding-dependent. Understanding precisely how the Rem/β interaction leads to channel endocytosis and decreased P_o is an interesting question for future experiments. It is tempting to speculate that Rem-induced reduction in Q_{max} (voltage sensor immobilization) underlies α_{1C}-binding-dependent inhibition of $Ca_V1.2$. Nevertheless, we cannot rule out that Rem binding to α_{1C}NT may also inhibit channel P_o using a parallel mechanism that is independent of voltage sensor immobilization. Such mechanistic details may potentially be resolved by evaluating the structural determinants on Rem necessary for α_{1C}-binding-dependent inhibition [16].

Over the last decade, several groups have investigated mechanisms of RGK GTPase inhibition of Ca_V channels, sometimes with discrepant results [10,11,12,16,21,31,35,36,37]. Often, across the various groups, these studies have involved different RGKs and distinct Ca_V1/Ca_V2 channel types, as well as varied experimental systems. This work produces the new insight that the mode of RGK-mediated Ca_V channel inhibition is customized at both the channel and GTPase level. Hence, a particular RGK can employ divergent mechanisms to block distinct Ca_V channel types, while a specific Ca_V channel isoform can be inhibited by different RGKs with diverse mechanisms. This perspective may help explain some of the inconsistent results previously published regarding RGK regulation of Ca_V channels.

In conclusion, this work contributes to the growing realization that the seemingly simple phenomenon of RGK inhibition of Ca_V1/Ca_V2 channels is underlain by a rich variety of mechanisms and structural determinants [16,36]. Such mechanistic complexity may be physiologically relevant as it could significantly enrich the functional versatility of RGKs as Ca^{2+} channel blockers in excitable cells. For example, RGK inhibition of I_{Ca} could occur on different timescales depending on the mode of block of Ca_V channels– β-binding-dependent decreases in N could lead to long-term reductions in current, while β-binding-independent regulation of Q_{max} produces short-term tuning of I_{Ca}. In-depth understanding of the complexities underlying RGK regulation of I_{Ca} will be important for deciphering such physiological dimensions of this channel modulation, and may be potentially exploited to create custom genetically encoded Ca_V channel blockers for specific applications.

Materials and Methods

cDNA cloning

XFP-tagged RGK constructs [mouse Rem (NM_009047); human Gem (NM_181702); human Rem2 (NM_173527); mouse Rad (NM_019662)] were generated by first polymerase chain reaction (PCR) amplifying and cloning XFP into pcDNA4.1 (Invitrogen) using *Kpn*I and *BamH*I sites. Subsequently, RGK constructs were PCR amplified and cloned downstream of XFP using *BamH*I and *EcoR*I sites. To generate CFP-Rem_{265}-$C1_{PKC\gamma}$, we used overlap extension PCR to fuse residues 26–89 of mouse PKCγ [38] to the C terminus of Rem_{265}. The fusion product was subsequently cloned downstream of CFP using *BamH*I and *EcoR*I sites. CFP-α_{1C} intracellular loops constructs were amplified by PCR and cloned downstream of the XFP molecule using *BamH*I and *EcoR*I sites. To generate XFP-tagged $Ca_V\beta$ constructs, we PCR amplified and cloned XFP into pAd CMV using *BamH*I and *Xba*I sites. $Ca_V\beta$s were amplified by PCR and cloned upstream of the XFP molecule using *Nhe*I and *BamH*I sites. Point mutations in β were generated using QuikChange Site-Directed Mutagenesis Kit (Stratagene). The thirteen-residue bungarotoxin binding site [BBS] [39] was engineered into the domain II S5–S6 extracellular loop of α_{1C} at residue 713 using unique restriction enzyme sites, *Stu*I and *BbrP*I. Primers that extended from the unique restriction sites were used together with primers containing the BBS sequence in an overlap extension PCR reaction. The overlap extension product was directly ligated into α_{1C}-YFP to generate α_{1C}[BBS]-YFP.

All PCR products were verified by sequencing

Cell culture and transfection. Low-passage-number HEK 293 cells (gift from Dr. Robert Kass, Columbia University) [40] were maintained in DMEM supplemented with 10% FBS and 100 μg ml^{-1} penicillin-streptomycin. HEK 293 cells cultured in 6-cm tissue culture dishes were transiently transfected with $Ca_V1.2\alpha_{1C}$ (6 μg), β_{2a} (6 μg), T antigen (2 μg), and the appropriate RGK construct (4 μg), using the calcium phosphate precipitation method. Cells were washed with PBS 5–8 h after transfection and maintained in supplemented DMEM. For confocal microscopy experiments, transfected HEK 293 cells were replated onto fibronectin-coated culture dishes with No. 0 glass coverslip bottoms (MaTek). For electrophysiology experiments cells were replated onto fibronectin-coated glass coverslips 24 h after transfection.

Electrophysiology

Whole-cell recordings were conducted 48–72 h after transfection using an EPC-8 or EPC-10 patch clamp amplifier (HEKA Electronics) controlled by PULSE software (HEKA). Micropipettes were fashioned from 1.5-mm thin-walled glass with filament (WPI Instruments), and filled with internal solution containing (in mM): 135 cesium methanesulphonate ($MeSO_3$), 5 CsCl, 5 EGTA, 1 $MgCl_2$, 4 MgATP (added fresh) and 10 HEPES (pH 7.3). Series resistance was typically 1.5–2 MΩ. There was no electronic series resistance compensation. External solution contained (in mM): 140 tetraethylammonium-$MeSO_3$, 5 $BaCl_2$, and 10 HEPES (pH 7.3). Whole-cell I–V curves were generated from a family of step depolarizations (−40 to +100 mV from a holding potential of −90 mV). Currents were sampled at 25 kHz and filtered at 5 or

10 kHz. Traces were acquired at a repetition interval of 6 s. Leak and capacitive currents were subtracted using a P/8 protocol.

Labeling of cell surface $Ca_V1.2$ channels with QD_{655}

Transfected cells were washed twice with PBS containing calcium and magnesium (pH 7.4, 0.9 mM $CaCl_2$ and 0.49 mM $MgCl_2$), and incubated with 1 μM biotinylated α-bungarotoxin in DMEM/3% BSA in the dark for 1 h at room temperature. Cells were washed twice with DMEM/3% BSA, and incubated with 10 nM streptavidin-conjugated QD_{655} for 1 h at 4°C in the dark. For confocal microscopy, cells were washed with PBS, and imaged in the same buffer. For flow cytometry, cells were harvested with trypsin, washed with PBS and assayed in the same buffer.

Confocal microscopy

Static images of α_{1C}[BBS]-YFP, XFP-Rem constructs and quantum dots signal were observed using a Leica TCS SPL AOBS MP Confocal microscope system and a 40× oil objective (HCX PL APO 1.25-.75 NA). HEK 293 cells expressing CFP/YFP fusion proteins were imaged using a 458/514-nm Argon laser line for excitation and red signals were imaged using a 633-nm helium-neon laser line for excitation.

Flow cytometry

Cells were counted using a BD LSRII Cell Analyzer. HEK 293 cells expressing CFP/YFP fusion proteins were excited at 407 and 488-nm, respectively, and red signal was excited at 633-nm. For each group of experiments we used isochronal untransfected and single color controls to manually set the appropriate gain settings for each fluorophore to ensure signals remained in the linear range and to set threshold values. The same gain settings were then used for assaying all isochronal transfection samples. Flow cytometry data were analyzed using FlowJo software.

Immunoprecipitation and immunoblotting

Confluent cultures of HEK 293 cells plated in 6-cm tissue culture dishes were harvested 48 h after transfection. Cells were washed in PBS and resuspended in 0.5 mL cold lysis buffer (50 mmol/L Tris-HCl, 150 mmol/L NaCl, 1% NP-40) containing 1× protease inhibitor cocktail for 30 minutes. Cell lysates were centrifuged at 10,000×g for 15 minutes at 4°C, and the supernatant precleared by incubation with 50 μL protein G beads slurry for 1 h. The mixture was centrifuged and the resulting supernatant incubated with 4 μg primary antibody [Santa Cruz Biotechnology: anti-Rem (SC58472); anti-Gem (SC19753); anti-Rem2 (SC160720); anti-Rad (SC49714)] and 50 μL protein G slurry for 1 h on a rotator. The mixture was again centrifuged, and the pellet washed four times with lysis buffer. 50 μL Laemmli sample buffer was added to the bead pellet and the mixture vortexed and heated (90°–100°C for 10 minutes). The sample was centrifuged and the supernatant loaded onto a gel for subsequent SDS-PAGE and Western blot analyses. For immunoblots, primary antibodies to GFP (Invitrogen, A6455) were detected by horseradish peroxidase-conjugated secondary antibodies (goat-anti rabbit obtained from Thermo Scientific, 32260) and enhanced chemiluminescence.

Fluorescence resonance energy transfer (FRET)

Determination of RGK-α_1 subunit intracellular domain interactions in live cells was accomplished using the three-cube FRET algorithm as previously described [27,28]. Cells transfected with XFP-tagged proteins were washed with Tyrode's solution and placed on an inverted microscope equipped for epifluorescence. Individual cells were excited using a 150-W Xenon arc lamp light source, and epifluorescence emission signals measured with a photomultiplier tube were integrated by a fluorometer and digitized. For each cell, three successive measurements were taken with filter cube sets optimum for measuring CFP, YFP, and FRET signals, respectively. Background and autofluorescence levels were determined by averages from single untransfected cells, and subtracted from experimental values from each cube. The FRET ratio (*FR*) was calculated from background-corrected experimental measurements as previously described [27,28].

Data and statistical analyses

Data were analyzed off-line using PulseFit (HEKA), Microsoft Excel and Origin software. Statistical analyses were performed in Origin using built-in functions. Statistically significant differences between means ($P<0.05$) were determined using two-tailed unpaired Student's *t* test. Data are presented as means ± S.E.M.

Supporting Information

Figure S1 Evidence that β_{TM} loses binding to Rem. (A) Confocal images of a HEK 293 cell co-expressing CFP-Rem_{265}-$C1_{PKC}$ and wild type YFP-β_3. Under basal conditions both CFP and YFP fluorescence are diffusely distributed in the cytosol. Upon addition of 1 μM PdBu (5 min), CFP-Rem_{265}-$C1_{PKC}$ is recruited to the nuclear and plasma membrane. The sub-cellular localization of YFP-β_3 dynamically follows that of CFP-Rem_{265}-$C1_{PKC}$, providing visual evidence of an interaction between the two proteins. Scale bar, 5 μm. (B) A mutant β_3 featuring three point mutations, YFP-β_{TM}, does not bind CFP-Rem_{265}-$C1_{PKC}$, as reported by the dynamic sub-cellular co-localization assay. (C) Co-immunoprecipitation assay indicates YFP-β_{2a} associates with CFP-Rem, and that this interaction is lost with YFP-β_{2aTM}.
(TIF)

Figure S2 Exemplar raw data from flow cytometry experiments used to determine the relative surface density of $Ca_V1.2$ channels. (A) Confocal images showing quantum dot labeling of cells transfected with α_{1C}[BBS]-YFP+β_{2a} ± CFP-Rem (*left*) and α_{1C}[BBS]-YFP+β_{2aTM} ± CFP-Rem (*right*). Images are reproduced from Fig. 2A, B. Scale bar, 25 μm. (B) Raw data from isochronal flow cytometry experiments showing fluorescence intensity of QD_{655} versus YFP signals for cells expressing α_{1C}[BBS]-YFP+β_{2a}+CFP-Rem (*left*) and α_{1C}[BBS]-YFP+β_{2aTM}+CFP-Rem (*right*). 50,000 cells were counted for each condition. Vertical and horizontal lines are threshold values set based on isochronal experiments using untransfected and single color control cells. Each dot represents a single cell. Dots have been arbitrarily color coded to facilitate visualization of distinct populations. Loosely, green dots represent α_{1C}[BBS]-YFP-positive cells that lack appreciable trafficking to the membrane (low QD_{655} signal), while red dots represent α_{1C}[BBS]-YFP-positive cells that display robust $Ca_V1.2$ channel trafficking to the surface (high QD_{655} signal). Black dots in the bottom left quadrant correspond to untransfected cells.
(TIF)

Figure S3 Histogram showing estimates of donor:acceptor ratio (N_D/N_A) for FRET experiments shown in Fig. 3.
(TIF)

Figure S4 Visual evidence that Rem selectively binds α_{1C} N-terminus. (A) Representative confocal images showing sub-cellular localization of YFP-tagged α_{1C} intracellular domains when expressed alone in HEK 293 cells. Aside from I–II loop,

which autonomously targets to the membrane and nucleus, all other α_{1C} intracellular domains show mostly diffuse distribution throughout the cell. Scale bar, 5 μm. (B) *Top row*, representative images of YFP-Rem demonstrate that this protein is membrane enriched when expressed in HEK 293 cells. *Bottom row*, representative images showing sub-cellular localization of CFP-tagged α_{1C} intracellular loops co-expressed with YFP-Rem. Only CFP-α_{1C}NT demonstrated redistribution from the cytosol to the plasma membrane when co-expressed with YFP-Rem. (C) Line scan analyses of CFP fluorescence from cells co-expressing YFP-Rem and CFP-tagged α_{1C} intracellular loops. Membrane localization of CFP-α_{1C}NT and CFP-α_{1C}I–II is evident from the sharp twin peaks of fluorescent signal separated by (cytoplasmic) regions with lower fluorescence intensity. Line scans were drawn to avoid the nucleus and areas with clustered fluorescence. (D) Relative membrane to cytosol fluorescence intensity ratios for CFP-tagged α_{1C} intracellular domains either expressed alone or together with YFP-Rem in HEK 293 cells. Absence of membrane targeting results in a ratio of one, while membrane localization/enrichment of a protein yields a ratio greater than one. By this analysis, only CFP-α_{1C}NT showed an increase in membrane localization when co-expressed with YFP-Rem. CFP-α_{1C}I–II showed a relative decrement in membrane localization when co-expressed with YFP-Rem, perhaps reflecting a competition for membrane binding sites.
(TIF)

Figure S5 Mapping the Rem binding site in α_{1C} N-terminus. (A) Schematic of α_{1C}NT peptide fragments used to map Rem binding site. (B) Co-localization pattern of specific YFP-tagged α_{1C} N-terminus fragments with CFP-Rem at the plasma membrane suggests Rem binds the distal end of α_{1C} N-terminus. Scale bar, 5 μm. (C) Relative membrane to cytosol fluorescence intensity ratios for YFP-tagged α_{1C}NT fragments co-expressed with CFP-Rem. Ratios greater than unity indicate membrane targeting/enrichment of fluorescence signal. Line scan analyses avoided the nucleus and clustered fluorescence signals from cytosolic areas.
(TIF)

Figure S6 Lack of interaction of Gem, Rem2, and Rad with α_{1C} N-terminus. (A) Confocal images of YFP-α_{1C}NT with CFP-tagged Gem, Rem2, and Rad show little co-localization. Scale bar, 5 μm. (B) Relative membrane to cytosol fluorescence intensity ratios for YFP-α_{1C}NT co-expressed with distinct CFP-tagged RGK proteins. (C) Co-immuoprecipitation assay to probe for α_{1C}NT interaction with Gem, Rem2, or Rad provides no evidence of an association.
(TIF)

Figure S7 Lack of interaction of Rad with α_{1C} intracellular loops. (A) Confocal images of mCherry-Rad and CFP-tagged α_{1C} intracellular loops and termini show no evidence of co-localization. Scale bar, 5 μm. (B) Relative membrane to cytosol fluorescence intensity ratios for YFP-tagged α_{1C} intracellular loops co-expressed with distinct mCherry-tagged Rad. (C) Co-immuno-precipitation assays indicate no interaction between Rad and the major α_{1C} intracellular loops.
(TIF)

Acknowledgments

The authors thank Ms. Ming Chen for excellent technical assistance.

Author Contributions

Conceived and designed the experiments: TY HMC. Performed the experiments: TY AP HMC. Analyzed the data: TY AP HMC. Wrote the paper: TY HMC.

References

1. Catterall WA, Few AP (2008) Calcium channel regulation and presynaptic plasticity. Neuron 59: 882–901.
2. Catterall WA (2000) Structure and regulation of voltage-gated Ca2+ channels. Annu Rev Cell Dev Biol 16: 521–555.
3. Evans RM, Zamponi GW (2006) Presynaptic Ca2+ channels–integration centers for neuronal signaling pathways. Trends Neurosci 29: 617–624.
4. Triggle DJ (2007) Calcium channel antagonists: clinical uses–past, present and future. Biochem Pharmacol 74: 1–9.
5. Kochegarov AA (2003) Pharmacological modulators of voltage-gated calcium channels and their therapeutical application. Cell Calcium 33: 145–162.
6. Kolosov A, Goodchild CS, Cooke I (2010) CNSB004 (Leconotide) causes antihyperalgesia without side effects when given intravenously: a comparison with ziconotide in a rat model of diabetic neuropathic pain. Pain Med 11: 262–273.
7. Valentino K, Newcomb R, Gadbois T, Singh T, Bowersox S, et al. (1993) A selective N-type calcium channel antagonist protects against neuronal loss after global cerebral ischemia. Proc Natl Acad Sci U S A 90: 7894–7897.
8. Anekonda TS, Quinn JF, Harris C, Frahler K, Wadsworth TL, et al. (2010) L-type voltage-gated calcium channel blockade with isradipine as a therapeutic strategy for Alzheimer's disease. Neurobiol Dis 41: 62–70.
9. Colicelli J (2004) Human RAS superfamily proteins and related GTPases. Sci STKE 2004: RE13. RE13.
10. Beguin P, Nagashima K, Gonoi T, Shibasaki T, Takahashi K, et al. (2001) Regulation of Ca2+ channel expression at the cell surface by the small G-protein kir/Gem. Nature 411: 701–706.
11. Chen H, Puhl HL, 3rd, Niu SL, Mitchell DC, Ikeda SR (2005) Expression of Rem2, an RGK family small GTPase, reduces N-type calcium current without affecting channel surface density. J Neurosci 25: 9762–9772.
12. Finlin BS, Crump SM, Satin J, Andres DA (2003) Regulation of voltage-gated calcium channel activity by the Rem and Rad GTPases. Proc Natl Acad Sci U S A 100: 14469–14474.
13. Wang G, Zhu X, Xie W, Han P, Li K, et al. (2010) Rad as a novel regulator of excitation-contraction coupling and beta-adrenergic signaling in heart. Circ Res 106: 317–327.
14. Chang L, Zhang J, Tseng YH, Xie CQ, Ilany J, et al. (2007) Rad GTPase deficiency leads to cardiac hypertrophy. Circulation 116: 2976–2983.
15. Flynn R, Zamponi GW (2010) Regulation of calcium channels by RGK proteins. Channels (Austin) 4: 434–439.
16. Yang T, Xu X, Kernan T, Wu V, Colecraft HM (2010) Rem, a member of the RGK GTPases, inhibits recombinant CaV1.2 channels using multiple mechanisms that require distinct conformations of the GTPase. J Physiol 588: 1665–1681.
17. Xu X, Colecraft HM (2009) Engineering proteins for custom inhibition of Ca(V) channels. Physiology (Bethesda) 24: 210–218.
18. Buraei Z, Yang J (2010) The {beta} Subunit of Voltage-Gated Ca2+ Channels. Physiol Rev 90: 1461–1506.
19. Dolphin AC (2003) Beta subunits of voltage-gated calcium channels. J Bioenerg Biomembr 35: 599–620.
20. Yang T, Suhail Y, Dalton S, Kernan T, Colecraft HM (2007) Genetically encoded molecules for inducibly inactivating CaV channels. Nat Chem Biol 3: 795–804.
21. Fan M, Buraei Z, Luo HR, Levenson-Palmer R, Yang J (2010) Direct inhibition of P/Q-type voltage-gated Ca2+ channels by Gem does not require a direct Gem/Cavbeta interaction. Proc Natl Acad Sci U S A 107: 14887–14892.
22. Crump SM, Correll RN, Schroder EA, Lester WC, Finlin BS, et al. (2006) L-type calcium channel alpha-subunit and protein kinase inhibitors modulate Rem-mediated regulation of current. Am J Physiol Heart Circ Physiol 291: H1959–1971.
23. Beguin P, Ng YJ, Krause C, Mahalakshmi RN, Ng MY, et al. (2007) RGK small GTP-binding proteins interact with the nucleotide kinase domain of Ca2+-channel beta-subunits via an uncommon effector binding domain. J Biol Chem 282: 11509–11520.
24. Fang K, Colecraft HM (2011) Mechanism of auxiliary beta-subunit-mediated membrane targeting of L-type (Ca(V)1.2) channels. J Physiol 589: 4437–4455.
25. Heo WD, Inoue T, Park WS, Kim ML, Park BO, et al. (2006) PI(3,4,5)P3 and PI(4,5)P2 lipids target proteins with polybasic clusters to the plasma membrane. Science 314: 1458–1461.
26. Correll RN, Pang C, Finlin BS, Dailey AM, Satin J, et al. (2007) Plasma membrane targeting is essential for Rem-mediated Ca2+ channel inhibition. J Biol Chem 282: 28431–28440.
27. Erickson MG, Alseikhan BA, Peterson BZ, Yue DT (2001) Preassociation of calmodulin with voltage-gated Ca(2+) channels revealed by FRET in single living cells. Neuron 31: 973–985.

28. Erickson MG, Liang H, Mori MX, Yue DT (2003) FRET two-hybrid mapping reveals function and location of L-type Ca2+ channel CaM preassociation. Neuron 39: 97–107.
29. Pang C, Crump SM, Jin L, Correll RN, Finlin BS, et al. (2010) Rem GTPase interacts with the proximal Ca(V)1.2 C-terminus and modulates calcium-dependent channel inactivation. Channels (Austin) 4.
30. Correll RN, Pang C, Niedowicz DM, Finlin BS, Andres DA (2008) The RGK family of GTP-binding proteins: regulators of voltage-dependent calcium channels and cytoskeleton remodeling. Cell Signal 20: 292–300.
31. Beguin P, Mahalakshmi RN, Nagashima K, Cher DH, Ikeda H, et al. (2006) Nuclear sequestration of beta-subunits by Rad and Rem is controlled by 14-3-3 and calmodulin and reveals a novel mechanism for Ca2+ channel regulation. J Mol Biol 355: 34–46.
32. Sasaki T, Shibasaki T, Beguin P, Nagashima K, Miyazaki M, et al. (2005) Direct inhibition of the interaction between alpha-interaction domain and beta-interaction domain of voltage-dependent Ca2+ channels by Gem. J Biol Chem 280: 9308–9312.
33. Dalton S, Takahashi SX, Miriyala J, Colecraft HM (2005) A single CaVbeta can reconstitute both trafficking and macroscopic conductance of voltage-dependent calcium channels. J Physiol 567: 757–769.
34. Correll RN, Botzet GJ, Satin J, Andres DA, Finlin BS (2008) Analysis of the Rem2 – voltage dependant calcium channel beta subunit interaction and Rem2 interaction with phosphorylated phosphatidylinositide lipids. Cell Signal 20: 400–408.
35. Finlin BS, Mosley AL, Crump SM, Correll RN, Ozcan S, et al. (2005) Regulation of L-type Ca2+ channel activity and insulin secretion by the Rem2 GTPase. J Biol Chem 280: 41864–41871.
36. Seu L, Pitt GS (2006) Dose-dependent and isoform-specific modulation of Ca2+ channels by RGK GTPases. J Gen Physiol 128: 605–613.
37. Xu X, Marx SO, Colecraft HM (2010) Molecular mechanisms, and selective pharmacological rescue, of Rem-inhibited CaV1.2 channels in heart. Circ Res 107: 620–630.
38. Oancea E, Teruel MN, Quest AF, Meyer T (1998) Green fluorescent protein (GFP)-tagged cysteine-rich domains from protein kinase C as fluorescent indicators for diacylglycerol signaling in living cells. J Cell Biol 140: 485–498.
39. Sekine-Aizawa Y, Huganir RL (2004) Imaging of receptor trafficking by using alpha-bungarotoxin-binding-site-tagged receptors. Proc Natl Acad Sci U S A 101: 17114–17119.
40. Tateyama M, Kurokawa J, Terrenoire C, Rivolta I, Kass RS (2003) Stimulation of protein kinase C inhibits bursting in disease-linked mutant human cardiac sodium channels. Circulation 107: 3216–3222.